Robotica (2006) volume 24, pp. 699–710. © 2006 Cambridge University Press
doi:10.1017/S0263574706002876 Printed in the United Kingdom

Series damper actuator system based on MR fluid damper

Chee-Meng Chew*, Geok-Soon Hong and Wei Zhou

Department of Mechanical Engineering, National University of Singapore, 9 Engineering Drive 1, Singapore 117576 (Singapore)

(Received in Final Form: May 2, 2006. First published online: July 3, 2006)

SUMMARY

In our recent work, we have proposed a novel force control actuator system called series damper actuator (SDA). We have since built an SDA system based on magneto-rheological fluid (MR) damper. In this paper, the dynamics property of SDA system based on the MR fluid damper (SMRDA) is investigated. The effect of the extra dynamics introduced by the MR fluid damper is revealed by comparing the SMRDA with the SDA system based on a linear Newtonian viscous damper (SNVDA). To linearize the constitutive property of the MR fluid damper, a modified Bingham model is proposed. A force feedback control loop is implemented after the linearization. An experimental SMRDA is built to illustrate the performance of the SDA system.

KEYWORDS: Series damper actuator; Series elastic actuator; Magneto-rheological fluid damper; Bingham model; Impedance; Force control.

1. INTRODUCTION

Force/torque control is necessary when robots need to interact with unknown environment. This is especially true for robotics system such as assembly manipulators, legged robots, haptic devices, and so on. To implement force (from here, "force" generally means "force/torque") control, a common method is to use the strain gauge setup to obtain the force signal.[2,3] The performance of this method is poor due to its low signal-to-noise ratio. Furthermore, because of its high structural stiffness, it is not suitable for biomimetic legged robots or haptic devices, which require their joints to be both compliant and precisely force-controlled.

Currently, the best solution for this problem is called series elastic actuator (SEA)[4,5] proposed by MIT Leg Laboratory. The key feature of this method is the introduction of a series elastic component (SEC) between the motor and the load, which consequently increase the compliance of the actuator interface. The output force, f_{load} is indirectly controlled by controlling the deformation (measured by a sensor) of the elastic component, given the elastic property. Figure 1 shows a schematic diagram of the SEA.

The primary advantages of the SEA are good force fidelity, low output impedance, tolerance to shock loading, and robustness to changing loads. However, the introduction of an elastic component in the system increases the order of the system and consequently, reduces the bandwidth of the system.[6] Furthermore, the selection of the elastic property for the SEC is mainly governed by the trade-offs among the force bandwidth, force range, and impact tolerance. Due to the fact that the elastic property is usually a constant (since it is difficult to achieve variable elastic property design), it is very hard to achieve good force fidelity at both low- and high-end range.

To overcome some of the shortcomings in the SEA, Zinn *et al*.[7] proposed a force control actuation approach called distributed macro-mini actuation. This approach employs a pair of actuators that are connected in parallel. One of them is used to realize the low-frequency torque generation and the other one is for the high frequency. The resulting system can increase the force bandwidth, and yet be able to reduce impact loads. However, the system is more complex and costlier due to the requirement of additional actuators.

In our recent work, we have proposed a novel force control actuator system called series damper actuator (SDA) (US Patent pending).[1,8,9] Having a similar structure as the SEA, the proposed SDA system, as shown in Fig. 2, uses damper to replace spring as the series component in the actuator system. SDA can achieve both good force fidelity and high compliance, which is desirable for applications like legged robotics, haptic devices, etc. The SDA system can also potentially be applied to achieve a wide range of force output if the damping constant of the series damper can be varied.[1] To realize the concept of SDA system, we have built an SDA system based on a magneto-rheological (MR) fluid damper.

Although our proposed SDA system originated from the concept of SEA, the experimental setup of our proposed SDA system has a similar structure as Furusho's force control actuator.[10,11,15] In Furusho's system, an MR fluid damper was also located in series between the motor and the load. By controlling the input current to the damper, the output torque of the actuator could be achieved. In spite of the structural similarity of our experimental system to the Furusho's system, a different approach for force control has been adopted in our work. In the latter, it is assumed that the output force is not dependent on the input/output relative velocity of the damper. The drive unit (motor) mainly acts as a velocity source to one end of the MR damper. The output force of their actuator system is controlled mainly by varying the current supply to the MR fluid damper, which will in turn alter the Coulomb friction behavior for the damper. The MR fluid damper is thus behaving more like a force clutch.

* Corresponding author. E-mail: chewcm@alum.mit.edu

https://doi.org/10.1017/S0263574706002876 Published online by Cambridge University Press

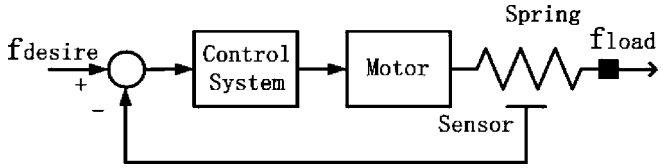


Fig. 1. Schematic diagram of SEA.

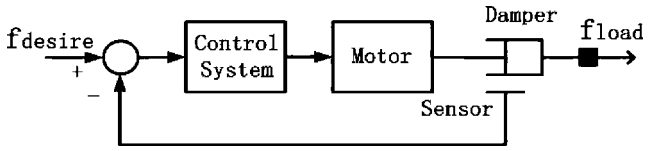


Fig. 2. Schematic diagram of SDA.

For our SDA system, the target damper is desirable to be of viscous type whose damping force is dependent on the damper's input/output relative velocity. If we know the constitutive property of the damper, the output force can be indirectly controlled by controlling the damper's input/output relative velocity. That is, the damper is acting like a force sensor. The MR damper in our actuator system is mainly used to emulate a viscous damper. In fact, the system can use a broad range of dampers, such as linear or nonlinear viscous damper, MR fluid damper, ER fluid damper, or other types of dampers, as long as their force output can be made to be a function of the input/output relative velocity (either by virtue of their designs or by software control).

In this paper, the dynamics property of the SDA system based on an MR fluid damper (SMRDA) is investigated. It is also compared with the SDA based on a linear Newtonian viscous damper (SNVDA). This paper is arranged as follows. The working principle of an SDA system is first introduced in Section 2. In Section 3, the properties of SMRDA and SNVDA are analyzed and compared through modeling. Section 4 presents the control algorithm for SMRDA. Finally, the experimental setup and results are described in Section 5, and Sections 6 and 7 provide discussion and conclusions.

2. SERIES DAMPER ACTUATOR

SDA system incorporates a series damper between the driver and the load. A schematic diagram of the SDA with a feedback loop is shown in Fig. 2. A typical SDA system consists of a control module, a driver, typically a motor with or without gear transmission; and a damper, typically viscous type. The output of the system is the force. This output variable is indirectly controlled by controlling the relative velocity of the damper given its damping coefficient. For a linear viscous damper, the output force can be known from the following equation:

$$F = bv, \tag{1}$$

where b is the damping coefficient and v is the relative velocity between the input and output ports of the damper.

Compared with the SEA system, the SDA system uses a series damping component instead of an elastic component and consequently, results in a system with system order being one less than that of SEA.[9] Hence, SDA will have a larger bandwidth than the SEA system. Another advantage of the SDA system is that the damping coefficient of the damper can easily be made variable by adopting an appropriate damper design, e.g., variable orifice viscous damper or MR fluid damper. This allows the damping coefficient to be adjusted according to the environment conditions. For example, at high force and low force ranges, the damping coefficient can be increased and decreased, respectively, to allow an appropriate relative velocity in the damper. This endows the system with higher force fidelity at both high and low force ranges. Furthermore, the SDA has inherent impact absorption property due to the energy dissipation property of the series damper. This characteristic is very important for walking robots, haptic devices, or robot manipulators to protect themselves from damage when they are subjected to external impact. The main disadvantage of using damper also comes from its energy dissipation property. Such a property limits the efficiency of the SDA system.[9]

For an ideal linear Newtonian viscous damper, the damping coefficient in Eq. (1) is a constant and the output force can be known from the velocity information of the damper if the damping constant is known in advance. However, if there is some error with the knowledge of damping coefficient, this error would directly reduce the output force fidelity because this error cannot be included in the velocity information. In this case, force sensor can be used here to measure the output force directly, rather than calculating the output force using velocity information based on Eq. (1). In most force control applications, the accuracy of the force control is usually not very crucial. The bandwidth property is usually more important. Hence, force control using velocity sensing is typically sufficient for most applications.

3. PROPERTY ANALYSIS FOR SDA

In this section, an investigation on the bandwidth (fixed end) and the output impedance of the SDA is carried out. An MR damper is adopted to be the series damper so that variable damping coefficient can be achieved. However, the MR fluid damper has more complex dynamics compared with the idea viscous damper as described by Eq. (1). To understand the effect of the extra dynamics of MR fluid damper, two different SDA models are studied and compared. One is the SNVDA model, in which the damping coefficient of the series damper is assumed to be constant and the output force is proportional to the damper's relative velocity. The other is the SMRDA model, which incorporates the extra dynamics introduced by the MR fluid damper. A comparison between SNVDA and SMRDA will be presented.

3.1. System models

3.1.1. Model of SNVDA. This section provides the model for the SNVDA system. The model and frequency domain block diagram for the SNVDA plant is shown in Fig. 3(a) and (b), respectively. To understand the force control properties of the SDA system, we investigate the SDA plants with a

https://doi.org/10.1017/S0263574706002876 Published online by Cambridge University Press

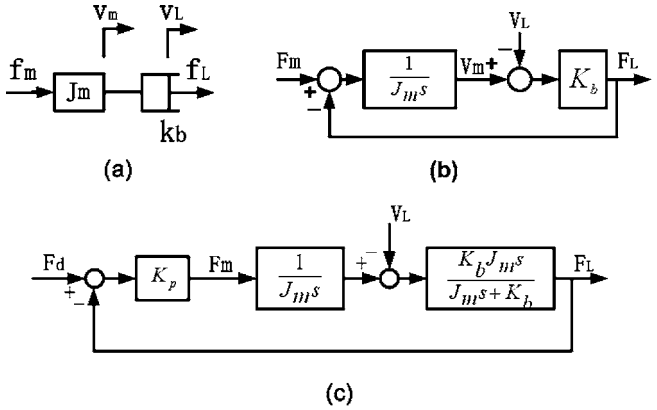


Fig. 3. (a) The SNVDA model; (b) the block diagram of SNVDA plant; and (c) the block diagram of the SNVDA system with a unit feedback and a proportional controller.

unity feedback and assume that a proportional control law is used for the feedback controller, as shown in Fig. 3(c). The adoption of such a simple control law is to enable the properties of this force control actuator system to be clearly illustrated. From the model, we can obtain the closed loop transfer function of the SNVDA system as follows:

$$F_{\mathrm{L}}(s) = \frac{K_{\mathrm{p}}K_{\mathrm{b}}F_{\mathrm{d}}(s) - K_{\mathrm{b}}J_{\mathrm{m}}sV_{\mathrm{L}}(s)}{J_{\mathrm{m}}s + K_{\mathrm{b}}(K_{\mathrm{p}}+1)}, \tag{2}$$

where K_{b} is the damping coefficient of the series damper; $V_{\mathrm{m}}(s)$ is the motor output velocity; $V_{\mathrm{L}}(s)$ is the load velocity; K_{p} is the proportional gain; $F_{\mathrm{L}}(s)$ is the load force; $F_{\mathrm{d}}(s)$ is the desired output force; $F_{\mathrm{m}}(s)$ is the force developed by the motor.

3.1.2. Model of SMRDA. Numerous mathematical models for the MR fluid damper have been proposed.[14] In this paper, a simple Bingham viscoplastic model is employed for the SMRDA system model (Fig. 4(a)). In this model, the behavior of the MR fluid damper can be expressed as follows[12]:

$$F = K_{\eta}V_{\mathrm{d}} + F_{\tau}\mathrm{sign}\,(V_{\mathrm{d}}), \tag{3}$$

where F is the output force of the MR fluid damper; F_{τ} is the magnetic field-dependent torque/force; K_{η} is the damping coefficient when no input current I is applied; and V_{d} is the damper velocity.

This is a static model and valid only for applications that do not require fast response. Since fast response is desirable for the SDA system, the dynamics of the MR fluid damper has to be considered in the model. The dynamics of the MR fluid damper is mainly due to the response of the magnetic field dependent force F_{τ} with respect to the input current I. It is assumed to be a first-order dynamics as given by the following transfer function[15]:

$$G_{\tau}(s) = \frac{F_{\tau}(I)}{I} = K_{\tau}\frac{\omega_{\tau}}{s+\omega_{\tau}}, \tag{4}$$

where K_{τ} and ω_{τ} are constants, representing the gain and bandwidth of the dynamics, respectively. The block diagram of this MR fluid damper model is shown in Fig. 4(b).

SMRDA plant comprises of two components, *viz.* an electrical motor and an MR fluid damper. The model of SMRDA plant is illustrated graphically in Fig. 5, where F_{m} is the force developed by the motor, J_{m} is the rotor inertia, V_{m} is motor rotor velocity, V_{L} is the load velocity, and F_{L} is the load force (output force). The dynamics of the motor is

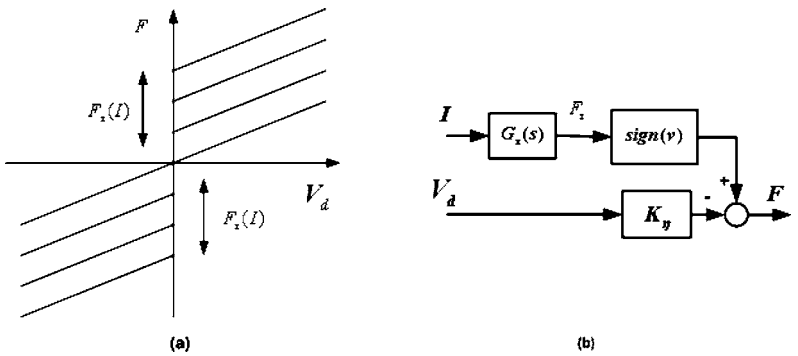


Fig. 4. Bingham viscoplastic model of MR fluid damper. (a) Force F vs. damper velocity V_{d} diagram. (b) Damper model block diagram.

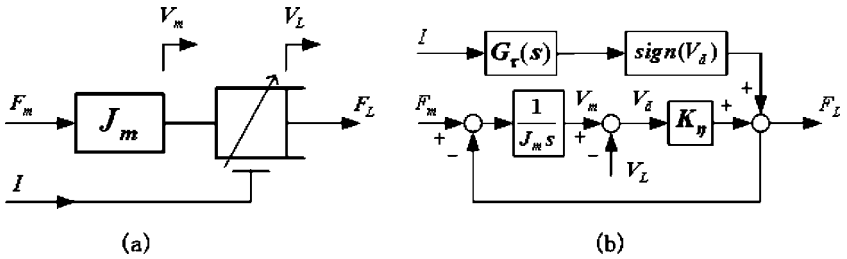


Fig. 5. (a) Schematic diagram of SMRDA structure. (b) SMRDA model block diagram.

https://doi.org/10.1017/S0263574706002876 Published online by Cambridge University Press

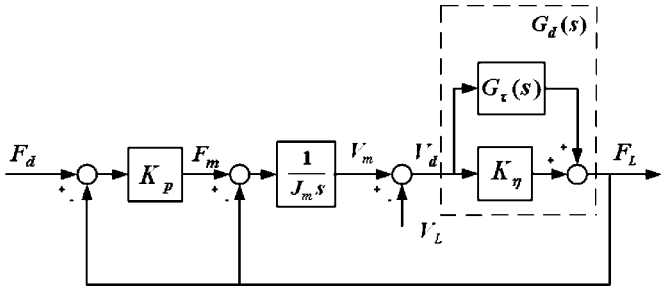


Fig. 6. The block diagram of the SMRDA system with proportional controller and unity feedback.

mainly due to the rotor inertia J_m as shown in Fig. 5(a). The block diagram of SMRDA plant is shown in Fig. 5(b).

To achieve force control in the SDA system, the damper is desired to possess linear constitutive property, that is, the force being proportional to the damper velocity V_d. Under static condition where F_τ is proportional to I, the linearity property can be achieved by using the following linearization algorithm for I:

$$I = K' V_\mathrm{d}. \tag{5}$$

Let us assume $K' = 1$. If the linearization algorithm is used and taking into account the dynamic behavior between F_τ and I (given by Eq. (4)), Eq. (3) becomes

$$F = K_\eta V_\mathrm{d} + K' G_\tau(s) V_\mathrm{d} = (K_\eta + G_\tau) V_\mathrm{d} = G_\mathrm{d} V_\mathrm{d}, \tag{6}$$

where G_d represents the MR fluid damper model after linearization and $G_\mathrm{d} = K_\eta + G_\tau$.

The resulting SDA plant is controlled by a proportional control law with unity feedback as shown in Fig. 6. The resulting transfer function of the SMRDA system is as follows:

$$F_\mathrm{L} = \frac{K_\mathrm{p}(G_\tau + K_\eta)}{J_\mathrm{m} s + (G_\tau + K_\eta)(K_\mathrm{p} + 1)} F_\mathrm{d} - \frac{J_\mathrm{m} s (G_\tau + K_\eta)}{J_\mathrm{m} s + (G_\tau + K_\eta)(K_\mathrm{p} + 1)} V_\mathrm{L}, \tag{7}$$

where F_d is the desired output force. Substituting Eq. (4) into the transfer function of SMRDA, Eq. (7) yields

$$F_\mathrm{L} = \frac{K_\mathrm{p} K_\eta s + K_\mathrm{p} \omega_\tau (K_\tau + K_\eta)}{J_\mathrm{m} s^2 + (J_\mathrm{m} \omega_\tau + K_\eta + K_\mathrm{p} K_\eta) s + (K_\mathrm{p} + 1)(K_\tau + K_\eta)\omega_\tau} F_\mathrm{d} - \frac{K_\eta J_\mathrm{m} s^2 + J_\mathrm{m} \omega_\tau (K_\tau + K_\eta) s}{J_\mathrm{m} s^2 + (J_\mathrm{m} \omega_\tau + K_\eta + K_\mathrm{p} K_\eta) s + (K_\mathrm{p} + 1)(K_\tau + K_\eta)\omega_\tau} V_\mathrm{L}. \tag{8}$$

3.2. Simulation and analysis

In this section, SMRDA was compared with SNVDA model in terms of the system bandwidth (fixed end) and the output impedance. The parameter values used for the simulations are listed in Table I. To make these two systems comparable, we assumed that $K_\eta + K_\tau = K_\mathrm{d}$. In the simulations, K_τ, K_η, and ω_τ are varied to show their effects on the system properties.

Table I. The parameter values used in the simulations.

Parameters	Values	Units
J_m	0.02	kg m^2
K_p	18.5	–
K_d	0.385	Nm s
K_τ	0–0.385	Nm s
K_η	0–0.385	Nm s
ω_τ	10–Inf.	rad/s

3.2.1. Bandwidth of SNVDA. According to Eq. (2), the transfer function of SNVDA, when output end is fixed, can be written as

$$\frac{F_\mathrm{L}}{F_\mathrm{d}} = \frac{K_\mathrm{p} K_\mathrm{d}}{J_\mathrm{m} s + K_\mathrm{d}(K_\mathrm{p} + 1)}. \tag{9}$$

That is, SNVDA can be described by a first-order model. Note that the introduction of the Newtonian viscous damper does not increase the order of the actuator system. Rewriting Eq. (9) gives

$$\frac{F_\mathrm{L}}{F_\mathrm{d}} = K' \frac{\omega_1}{s + \omega_1}, \tag{10}$$

where

$$K' = \frac{K_\mathrm{p}}{K_\mathrm{p} + 1},$$

and

$$\omega_1 = \frac{K_\mathrm{d}(K_\mathrm{p} + 1)}{J_\mathrm{m}}. \tag{11}$$

For a first-order system described by Eq. (10), ω_1 is the bandwidth of this actuator system. The Bode magnitude plot of Eq. (10) is shown in Fig. 7.

3.2.2. Output impedance of the SNVDA system. The output impedance, sometimes also called the mechanical

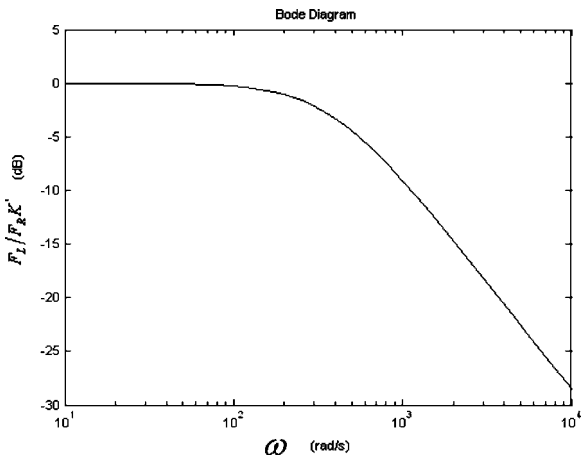


Fig. 7. Bode magnitude response of the SNVDA actuator system.

https://doi.org/10.1017/S0263574706002876 Published online by Cambridge University Press

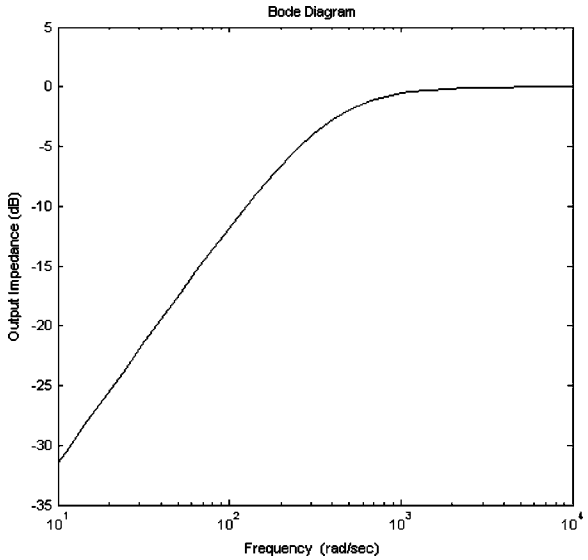


Fig. 8. The output impedance of the SNVDA system.

impedance, is defined as

$$Z(s) = \frac{F_e(s)}{V_L(s)}, \tag{12}$$

where V_L represents the velocity at the load end, $F_e(s)$ ($F_e(s) = -F_L(s)$) represents the external force exerted on the output end of the actuator due to the load movement.

Low output impedance is a desirable property for the SDA system. From Eq. (2), the output impedance of the SNVDA system is

$$Z(s) = \frac{K_d J_m s}{J_m s + K_d(K_p + 1)}. \tag{13}$$

Normalizing the equation with the damping constant K_d, we have

$$Z'(s) = \frac{F_e}{V_L K_d} = \frac{J_m s}{J_m s + K_d(K_p + 1)} = \frac{s}{s + \omega_1}. \tag{14}$$

The output impedance of SNVDA system is plotted against the frequency in Fig. 8. It is observed that the output impedance at low frequency is low (which is desirable). When the frequency is higher than the SNVDA system's bandwidth ω_1, the output impedance approaches the damping constant K_d.

3.2.3. Bandwidth of SMRDA system. According to Eq. (8), the transfer function of SMRDA can be expressed as

$$\frac{F_L}{F_d} = \frac{K_p K_\eta s + K_p \omega_\tau (K_\eta + K_\tau)}{J_m s^2 + (J_m \omega_\tau + K_p + K_p K_\eta)s + (K_\tau + K_\eta)(K_p + 1)\omega_\tau}. \tag{15}$$

Note that the dynamics of the MR fluid damper increases the order of the actuator system. Higher order usually means lower bandwidth and narrower stability margin. K_η and K_τ are the gains of Newtonian viscous component and field-dependent component in the MR fluid damper dynamics, respectively, as described in Eqs. (3) and (4). To know their effects on the property of the SDA system, the values of K_η and K_τ are varied in the simulation. Different values of K_η and K_τ represent different proportions of the extra dynamics (field-dependent component) caused by MR fluid in the whole dynamics of damper. Two extreme conditions are analyzed. The first is achieved by setting $K_\eta = K_d$ and $K_\tau = 0$. This corresponds to the case where the extra dynamics of the MR fluid damper becomes negligible. The other is achieved by setting $K_\eta = 0$ and $K_\tau = K_d$. This corresponds to the case where the extra dynamics is significant.

Case A: $K_\eta = K_d$ and $K_\tau = 0$:

Under this condition, Eq. (15) can be further simplified as follows:

$$\frac{F_L}{F_d} = \frac{K_p K_\eta}{J_m s + K_\eta(K_p + 1)}. \tag{16}$$

In this case, the transfer function is identical to that of SNVDA (Eq. (9)). So the bandwidth of SMRDA is given by Eq. (11). This is because the MR fluid damper behaves like a Newtonian viscous damper when there is no magnetic field-dependent component in Eq. (3).

Case B: $K_\eta = 0$ and $K_\tau = K_d$:

In this case, Eq. (15) can be modified as follows:

$$\frac{F_L}{F_d} = \frac{K_p K_\tau \omega_\tau}{J_m s^2 + J_m \omega_\tau s + K_\tau(K_p + 1)\omega_\tau}. \tag{17}$$

The system transfer function is rewritten as follows:

$$\frac{F_L}{F_d} = K' \frac{\omega_2^2}{s^2 + 2\xi\omega_2 s + \omega_2^2},$$

where

$$K' = \frac{K_p}{K_p + 1},$$

$$\omega_2 = \sqrt{\frac{K_\tau(K_p + 1)\omega_\tau}{J_m}},$$

and

$$\xi = \frac{1}{2}\sqrt{\frac{J_m \omega_\tau}{K_\tau(K_p + 1)}}.$$

In this case, the model is a typical second-order system. Here, ω_2 and ξ are the undamped natural frequency and the damping ratio, respectively of this system. The system bandwidth is dependent on both parameters.[a]

Now, let us consider the effect of ω_τ on the system bandwidth. When $\omega_\tau \to 0$, the system bandwidth tends to zero. If $\omega_\tau \to \infty$, Eq. (17) can be rewritten as

$$\frac{F_L}{F_d} = \frac{K_p K_\tau}{(J_m/\omega_\tau)s^2 + J_m s + K_\tau(K_p + 1)} \cong \frac{K_p K_\tau}{J_m s + K_\tau(K_p + 1)}.$$

[a] For this second-order system, Bandwidth $= \omega_2\sqrt{2\sqrt{\xi^4 - \xi^2 + 1} - 2\xi^2 + 1}$.

https://doi.org/10.1017/S0263574706002876 Published online by Cambridge University Press

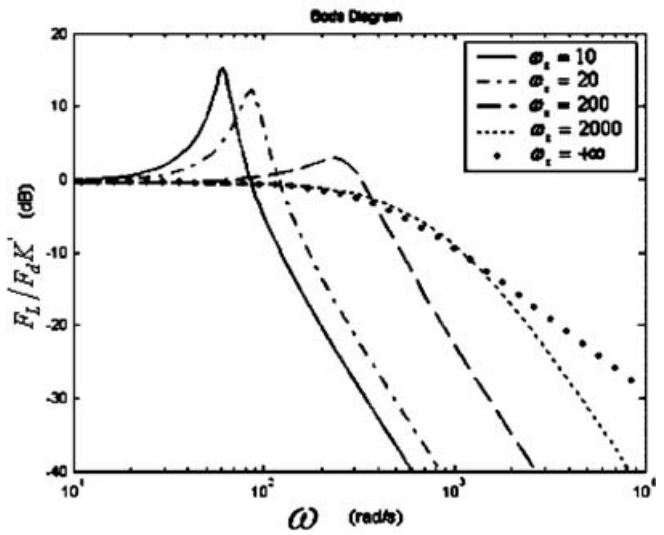


Fig. 9. Bode magnitude plot of the SMRDA system with different value of ω_τ, when $K_\eta = 0$ and $K_\tau = K_\mathrm{d}$.

This transfer function equals to that of SNVDA. When ω_τ approaches infinity, the current input response dynamics of the MR fluid damper (Eq. (4)), behaves like a zero-order system with constant gain K_τ.

The Bode plot of the SMRDA system for different ω_τ is shown in Fig. 9. It is observed that the bandwidth of the SMRDA system increases with the increase of ω_τ in the low-end range. As ω_τ is large, the bandwidth of the SMRDA system approaches that of the SNVDA system as defined in Eq. (11). If ω_τ is large enough, the high-order dynamics introduced by the MR fluid damper can be neglected. However, the typical value of ω_τ for the MR fluid damper is usually in the low-end range. Hence, the extra dynamics introduced by the MR fluid damper is usually not negligible, and will inevitably reduce the bandwidth of the overall system.

The two cases discussed earlier are the extreme cases. Figure 10 shows the simulation results of the SMRDA

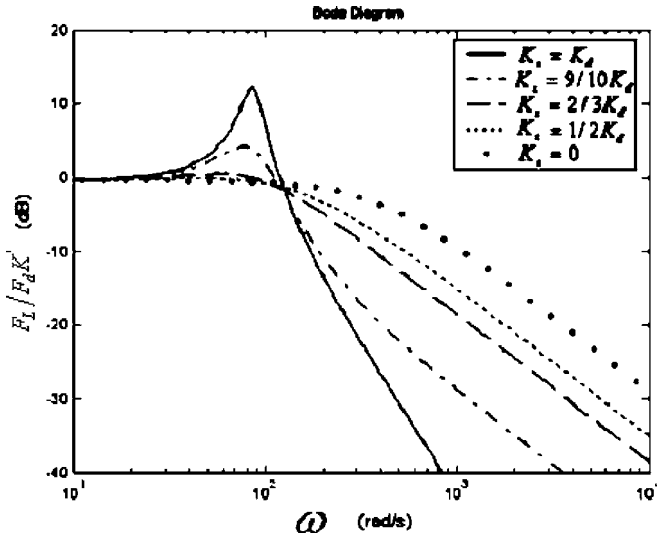


Fig. 10. Bode magnitude plot of SMRDA system with different value of K_τ, when $\omega_\tau = 20$ rad/s and $K_\tau + K_\eta = K_\mathrm{d}$.

systems with different proportions of Newtonian viscous component K_η and field-dependent component K_τ, when $K_\tau + K_\eta \equiv K_\mathrm{d}$ and $\omega_\tau = 20$ rad/s (20 rad/s is a typical value for the MR fluid damper used). It is shown that the transfer function, and therefore, the bandwidth of the SMRDA system is always between the first-order system described by Eq. (16) and the second-order system described by Eq. (17). If the ratio of K_τ over K_η increases, the system model approaches the second-order system and the bandwidth reduces. On the contrary, if the ratio of K_τ over K_η decreases, the system model approaches the first-order system and the bandwidth increases.

3.2.4. Output Impedance of the SMRDA system. From Eq. (8), the output impedance of the SMRDA system is

$$Z(s) = \frac{K_\eta J_\mathrm{m} s^2 + J_\mathrm{m}\omega_\tau(K_\tau + K_\eta)s}{J_\mathrm{m}s^2 + (J_\mathrm{m}\omega_\tau + K_\eta + K_\mathrm{p}K_\eta)s + (K_\mathrm{p}+1)(K_\tau + K_\eta)\omega_\tau}. \tag{18}$$

To compare with the SNVDA system, the output impedance equation is normalized with the damping coefficient $(K_\tau + K_\eta)$ as follows:

$$Z'(s) = \frac{F_\mathrm{e}}{V_\mathrm{L}(K_\tau + K_\eta)} = \frac{(K_\eta/(K_\tau + K_\eta))J_\mathrm{m}s^2 + J_\mathrm{m}\omega_\tau s}{J_\mathrm{m}s^2 + (J_\mathrm{m}\omega_\tau + K_\eta + K_\mathrm{p}K_\eta)s + (K_\mathrm{p}+1)(K_\tau + K_\eta)\omega_\tau}. \tag{19}$$

As in the previous section, two extreme cases are considered here: $K_\eta = K_\mathrm{d}, K_\tau = 0$; and $K_\eta = 0, K_\tau = K_\mathrm{d}$.

Case A: $K_\eta = K_\mathrm{d}, K_\tau = 0$:

In this case, Eq. (19) can be written as

$$Z'(s) = \frac{J_\mathrm{m}s}{J_\mathrm{m}s + K_\eta(K_\mathrm{p}+1)}.$$

The resulting function is similar to that of the SNVDA system (Eq. (13)) because the SMRDA system behaves like the SNVDA system when $K_\eta = K_\mathrm{d}, K_\tau = 0$.

Case B: $K_\tau = 0, K_\eta = K_\mathrm{d}$:

In this case, the output impedance Eq. (19) can be written as

$$Z'(s) = \frac{J_\mathrm{m}\omega_\tau s}{J_\mathrm{m}s^2 + J_\mathrm{m}\omega_\tau s + K_\tau(K_\mathrm{p}+1)\omega_\tau}.$$

To consider the effect of ω_τ on $Z'(s)$, the output impedance was plotted against ω_τ as shown in Fig. 11. Similar to the SNVDA system, the output impedance of the SMRDA system is also low when the frequency is low. The output impedance magnitude reaches its peak value around the system high cutoff frequency whose value is dependent on the value of ω_τ. However, being different from the SNVDA system, the output impedance reduces continuously and maintains low value when the frequency approaches infinity. That is, the system has low output impedance in both the low- and high-frequency range.

Figure 12 shows the output impedance for different values of K_η and K_τ when $\omega_\tau = 20$ rad/s, which is a typical value for the MR fluid damper. It is observed that the final value of

https://doi.org/10.1017/S0263574706002876 Published online by Cambridge University Press

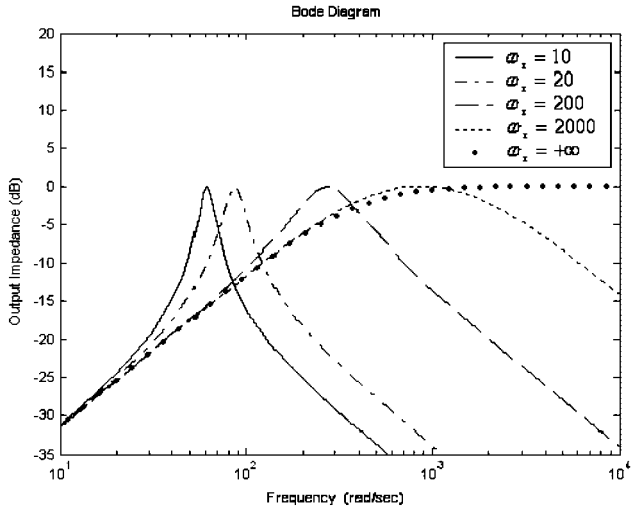


Fig. 11. Output impedance of the SMRDA system with different value of ω_τ, when $K_\eta = 0$ and $K_\tau = K_\mathrm{d}$.

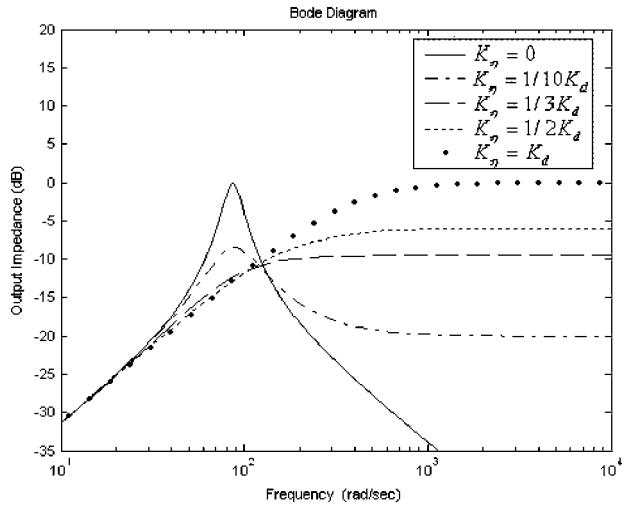


Fig. 12. Output impedance of the SMRDA system with different values of K_η and K_τ when $\omega_\tau = 20$ rad/s.

the output impedance described in Eq. (18) approaches K_η rather than K_d as in the case of the SNVDA system when the frequency approaches infinity.

The analyses showed that the introduction of the MR fluid damper into the SDA system increases the order of the system. The low-bandwidth ω_τ of the MR fluid damper response to the input current would compromise on the overall bandwidth of the SDA system. Therefore, to achieve large bandwidth for the SMRDA system, a large value for ω_τ is desirable.

It was also shown that the dynamics of the MR fluid damper causes the output impedance of SDA system to be low at both low- and high-frequency range. The output impedance reaches the maximum value around the system high cutoff frequency. When the frequency approaches infinity, the output impedance of the SMRDA system approaches the value of K_η, the Newtonian viscous component of the MR fluid damper. To reduce the output impedance at high frequency, a small K_η is desirable. However, a small K_η, which usually means a large ratio of K_τ to K_η, makes the SMRDA system more susceptible to the dynamics of the MR fluid damper especially when the value of ω_τ is low.

4. CONTROLLER DESIGN

In this section, the control algorithm for the SDA system based on the MR fluid damper is described. Due to the typical nonlinearity property of the MR fluid damper, the MR fluid damper would first be linearized using appropriate inverse models. After linearization, a closed loop controller is designed to achieve the force control for the system.

To linearize the MR fluid damper, an intuitive way is to employ inverse dynamics model as shown in Fig. 13. In the following sections, two dynamic models for the MR fluid damper will be presented and compared.

4.1. Dynamic models for MR fluid damper

In this section, we will consider two different models for the MR fluid damper. One of them is the Bingham viscoplastic model presented in Section 3.1.2. The Bingham model can be represented by the following equations:

$$F = f_0 \mathrm{sign}\,(V_\mathrm{d}) + c_0 V_\mathrm{d}, \tag{20}$$

$$f_0 = f_\mathrm{a} + f_\mathrm{b} I, \tag{21}$$

$$c_0 = c_\mathrm{a} + c_\mathrm{b} I, \tag{22}$$

where $f_\mathrm{a}, f_\mathrm{b}, c_\mathrm{a}, c_\mathrm{b}$ are model parameters; f_0 and c_0 are model internal variables; F, V_d, and I are the output force, the damper velocity, and the damper input current, respectively.

To achieve a better result, we propose a revised Bingham model as follows:

$$F = f_0 \mathrm{sign}\,(V_\mathrm{d})(1 - \exp\,(-\alpha abs(V_\mathrm{d}))) + c_0 V_\mathrm{d} + \beta, \tag{23}$$

$$f_0 = f_\mathrm{a} + f_\mathrm{b} P, \tag{24}$$

$$c_0 = c_\mathrm{a} + c_\mathrm{b} P, \tag{25}$$

$$\dot{P} = \gamma(I - P), \tag{26}$$

where $f_\mathrm{a}, f_\mathrm{b}, c_\mathrm{a}, c_\mathrm{b}, \alpha, \beta, \gamma$ are model parameters; f_0, c_0, P are model internal variables; F and V_d are the output force and the damper velocity, respectively.

In this new model, the extra first-order dynamics (represented by $G_\tau(s)$ in Section 3.1.2) in the MR fluid

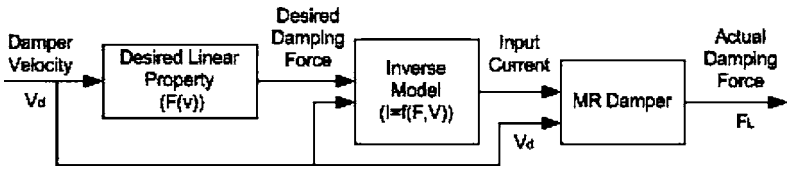


Fig. 13. Inverse dynamics control for MR fluid damper linearization.

https://doi.org/10.1017/S0263574706002876 Published online by Cambridge University Press

Table II. Values of model parameters.

	Units	Model 1	Model 2
f_a	Nm	0.1409	0.2803
f_b	Nm/A	2.5680	3.5394
c_a	Nm s	0.0163	−0.0120
c_b	Nm s/A	0.0057	0.0011
α	s	–	0.6641
β	Nm	–	−0.0612
γ	rad/s	–	16.4154

damper is modeled by Eq. (26). Another point to note is that the original Bingham model does not consider the hysteresis effect of the MR fluid damper. Therefore, significant error may result if this model is used. This error will also result in errors in the parameters identification (using the least square method). In the new model, the term $(1 - \exp(-\alpha abc(V_d)))$ in Eq. (23) helps to reduce the model error due to the hysteresis effect, and hence, results in a more accurate result during parameters identification.

Let us denote Model 1 and Model 2 for the origin Bingham model described by Eqs. (20)–(22) and the proposed modified model described by Eqs. (23)–(26), respectively. Using the nonlinear least square method, the values of the parameters in Eqs. (20)–(22) and (23)–(26) can be determined for the MR fluid damper. Table II shows a set of the parameters' values identified for our MR fluid damper used in the experimentation based on Model 1 and Model 2.

In Eq. (26), γ is the bandwidth of the MR fluid damper response to the input current. It is the same as ω_τ, which was used to denote the bandwidth of the MR fluid damper's extra dynamics $G_\tau(s)$ in Eq. (4). Identification results show a low value of γ, which will, according to the analysis of Section 3, compromise the overall bandwidth of SDA system. In fact, the low-bandwidth performance of the SDA system, which adopted MR fluid damper, has been reported in our previous works.[1,16]

4.2. Models validation for MR fluid damper

To validate the models, the predicted forces of Model 1 and Model 2, given the damper velocity and current, are compared with the measured MR fluid damper force. In this experiment, the MR damper was subjected to predetermined profiles for the relative velocity and the current, the actual output force (torque) was then measured. After that, the predicted forces were calculated using the same profiles for the relative velocity and the current, and compared with the actual output force as shown in Fig. 14. It can be seen that Model 2 gives a better damper response prediction. The response delay caused by the extra dynamics of MR fluid damper has been effectively compensated.

4.3. Linearization of MR fluid damper constitutive property

Based on Model 1 and Model 2, the MR fluid damper's constitutive property can be linearized using the approach depicted in Fig. 13. In this linearization algorithm, the desired

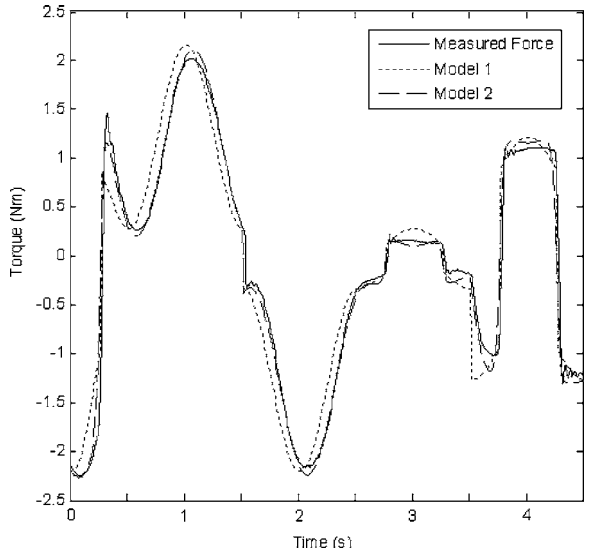


Fig. 14. Comparison between the experimental output force and predicted output force based on the two models.

linear property is defined as

$$F_{\text{desired}} = K_{\text{desired}} \times V_d, \tag{27}$$

where F_{desired} is the desired damping force, K_{desired} is the desired damping constant, and V_d is the damper velocity. The inversed modified Bingham model, based on Eqs. (23)–(26) can be written as

$$I = P + \frac{\dot{P}}{\gamma}, \tag{28}$$

$$P = \frac{F_{\text{desired}} - f_a \text{sign}(V_d)\left(1 - e^{-\alpha|V_d|}\right) - c_a V_d - \beta}{f_b \text{sign}(V_d)\left(1 - e^{-\alpha|V_d|}\right) + c_b V_d}. \tag{29}$$

With the linearization algorithm, the MR fluid damper output for the sinusoidal and the step inputs (for both models) are shown in Figs. 15 and 16, respectively. It is observed that the force output for Model 2 has a better phase matching and

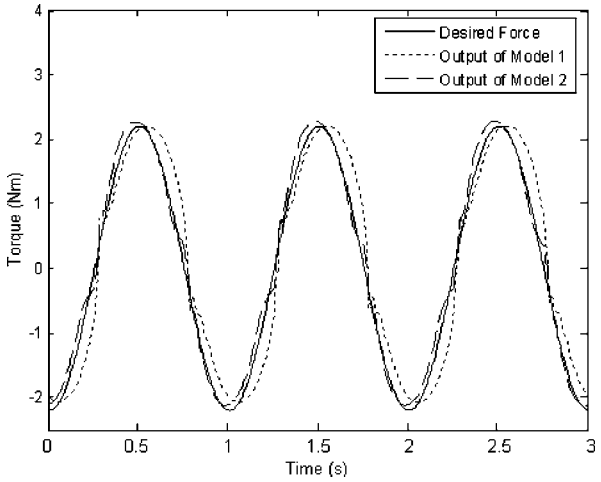


Fig. 15. Force outputs of MR fluid damper after linearization (open loop), for Models 1 and 2, where desired force is sinusoidal (for $K_d = 0.17$ Nm s).

https://doi.org/10.1017/S0263574706002876 Published online by Cambridge University Press

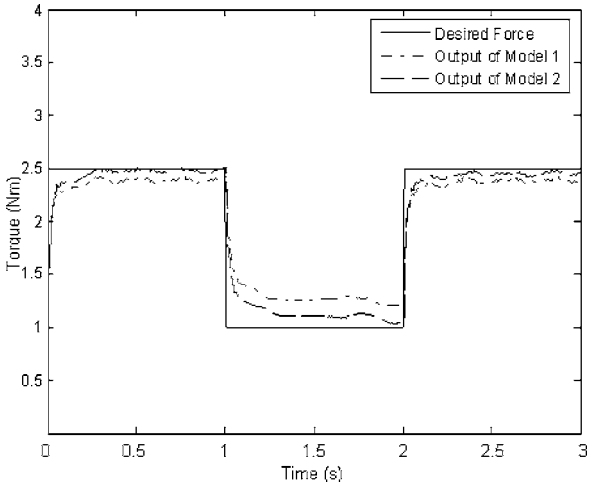


Fig. 16. Force outputs of MR fluid damper after linearization (open loop), for Models 1 and 2, where desired force is a square signal (for $K_d = 0.17$ Nm s).

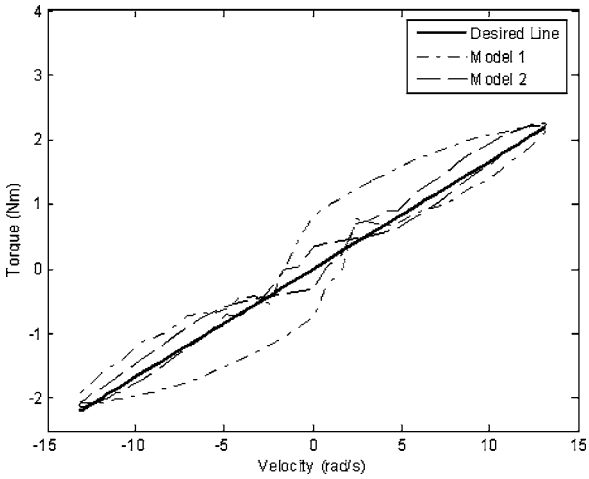


Fig. 17. Linearity properties comparison for MR fluid damper after linearization (open loop) using Models 1 and 2 (for $K_d = 0.17$ Nm s).

faster step response while the force output for Model 1 has a certain phase lag and a slower step response.

Due to the larger model identification error, Model 1 has a more inferior performance than Model 2. It can be seen from Fig. 17 that the MR fluid damper after linearization has a better linearity property for Model 2 than that for Model 1. The result based on Model 1 has also significant hysteresis behavior.

Figure 18 shows the Bode plots (corresponds to G_d in Fig. 13) of the MR fluid damper after the linearization based on Model 1 and Model 2, respectively. For Model 1, the damper, rather than working as a constant gain, shows a high-order dynamics character, which is caused by the extra dynamics of MR fluid and its linearization process. In Model 2, this extra dynamics is considered as a first-order model and compensated by the inverse model. Therefore, it gives a better frequency response, that is, a larger bandwidth and a small phase shifting as shown in Fig. 18.

Due to the better description of the MR fluid damper's actual dynamics, the proposed modified Bingham model gives a better performance after the linearization algorithm.

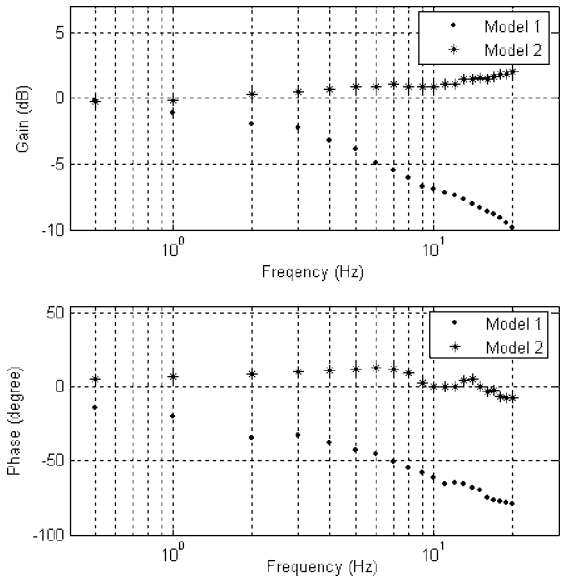


Fig. 18. Bode plots (G_d) of MR fluid damper after linearization, based on Models 1 and 2.

4.4. Overall control scheme for SMRDA

Theoretically, if the damping constant is known, the output force of the damper can be controlled by controlling the damper velocity. However, the output force fidelity is directly affected by the uncertainty in the actual damping constant. Although the MR fluid damper after the linearization has a good linear behavior, there are still deviations as shown in Fig. 17. To obtain a better performance for the SDA system, a force feedback control loop is implemented based on a force sensor.

When we analyze the SDA system in Section 3, we assume a simple proportional controller so that some fundamental properties of the system can be clearly illustrated. To achieve a better force control performance, a PID control scheme is used to control the SDA as shown in Fig. 19. The PID controller can be represented by following equation:

$$F_m = K_p e + K_I \int e + K_D \dot{e}, \tag{30}$$

where F_m represents the input signal for the motor and e is the error signal (difference between the reference signal (F_d) and the feedback signal (F_l)).

In Fig. 19, G_d represents the dynamics of the MR fluid damper after the linearization. The transfer function of G_d can be obtained from two different methods, *viz*. the theoretical method as shown in Section 3.1.2 and the experimental method obtained from Bode plot as shown in Fig. 18.

5. EXPERIMENTAL SETUP AND RESULTS

An experimental setup of the SMRDA and its schematic diagram are shown in Figs. 20 and 21, respectively. In this experimental system, two angular encoders are used to obtain the series damper's input angular velocity and output angular velocity, respectively. The relative angular velocity in the series damper, V_d, is then calculated from the difference between the two angular velocities.

https://doi.org/10.1017/S0263574706002876 Published online by Cambridge University Press

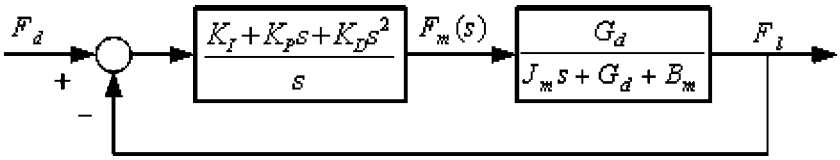


Fig. 19. Overall control scheme for SMRDA.

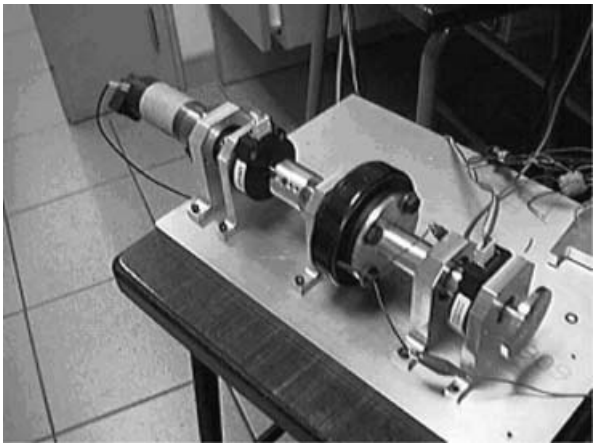


Fig. 20. Photograph of the experimental SMRDA.

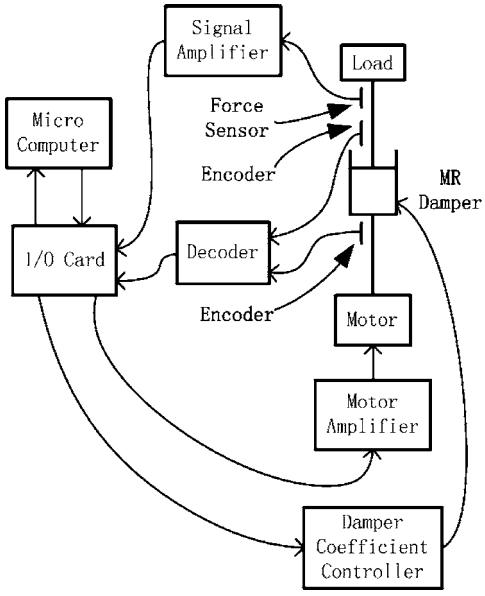


Fig. 21. Schematic diagram of the experimental system.

The series damper component is a commercial magneto-rheological fluid damper (Lord MRB-2107–3). A damping coefficient controller is used to control the input current (through a current amplifier) for the MR fluid damper according to the damper's linearization law. A force sensor is mounted at the output of the actuator to measure the actual system output force.

The main controller is implemented on a microcomputer system. It obtains the feedback signals from the force sensor and the two encoders, and computes the motor drive signal and MR fluid damper current according to the given control scheme so that the desired force can be achieved at the actuator output.

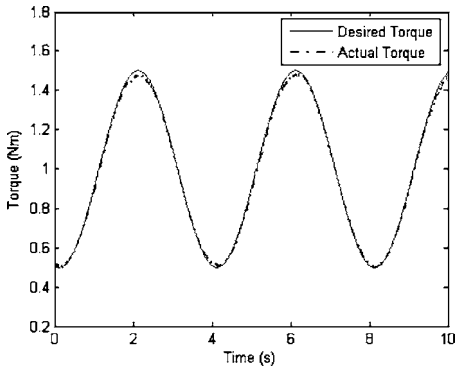


Fig. 22. Force tracking following a sinusoidal reference when the damping constant $K_d = 0.17$ Nm s.

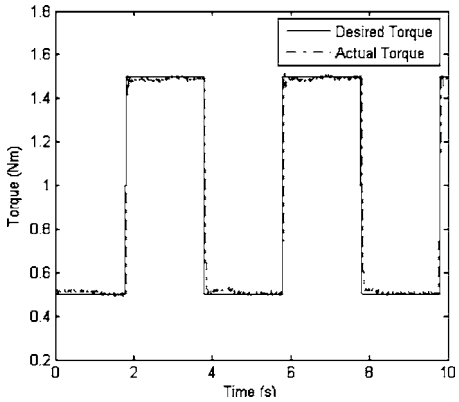


Fig. 23. Force tracking following a step reference when the damping constant $K_d = 0.17$ Nm s.

The results of the fixed-end experiment are shown in Figs. 22–26. Figures 22 and 23 illustrate the system responses to sinusoidal and step references, respectively (for $K_b = 0.17$ Nm s). The results show that the experimental SDA system can achieve good force fidelity. Comparing with the open loop outputs of the MR fluid damper after linearization (Figs. 15 and 16), the force tracking error is greatly reduced with the force feedback control loop.

As explained in Section 2, being able to achieve variable damping coefficient is an advantage of the SDA system. To illustrate this advantage using the experimental setup, the system responses for sinusoidal and square inputs, respectively, are obtained (see Figs. 24 and 25) when the desired damping constant K_d of the series damper has been doubled to $K_d = 0.34$ Nm s, while the amplitudes of the inputs were increased four times. Comparing Figs. 23 and 25, we can observe no significant deterioration in force tracking even when the latter amplitude was increased four times.

Figure 26 shows the force tracking result for a sinusoidal reference, which goes across zero. It shows that there is some

https://doi.org/10.1017/S0263574706002876 Published online by Cambridge University Press

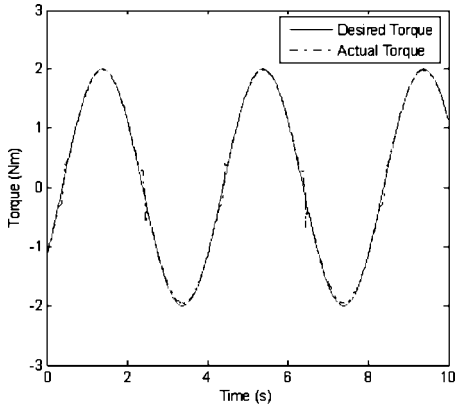


Fig. 24. Force tracking following a sinusoidal reference when the damping constant $K_d = 0.34$ Nm s.

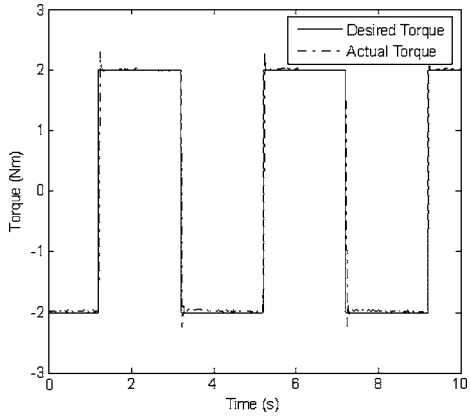


Fig. 25. Force tracking following a step reference when the damping constant $K_d = 0.34$ Nm s.

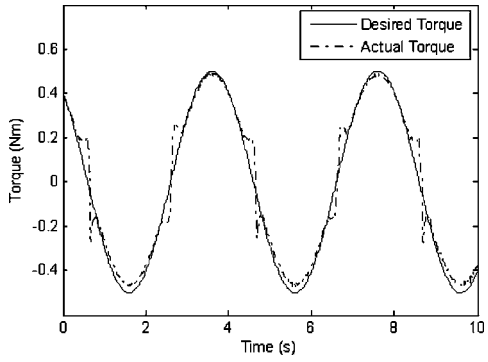


Fig. 26. Force tracking for small amplitude sinusoidal reference, which goes across zero.

unexpected output force tracking error when the damper velocity is ready to cross zero. Such error is not observed when the output is always above or below zero as shown in Fig. 22. This range is around ±0.2 Nm. It is less than 10% of the maximum output range which is ±3 Nm. This error may be due to the hysteresis or Coulomb friction effect of the MR fluid damper. Such effects are not modeled and compensated in the proposed algorithm. Using some hysteresis type model, such as Bouc-Wen model,[14] and better lubrication to reduce such frictional effect, this problem can be minimized.

6. DISCUSSION

The main difference between the SDA-based force control implementation and the existing MR fluid damper-based force control implementation[10,11] is that the latter assumes that the output force is not dependent on the input/output relative velocity of the damper. The drive unit is mainly used to supply a velocity source to one end of the MR fluid damper. The output force is only controlled by the current supplied to the MR fluid damper.

For the SDA system, the series damper is assumed to have known output force versus damper's velocity (relative velocity between the input and output ends) relationship. So, no matter whether the relationship is linear or not, as long as it is invertible, the output force can be achieved by directly controlling the damper's velocity. Therefore, the SDA system can use a broad range of dampers, such as linear or nonlinear viscous damper, MR fluid damper, ER fluid damper, or other types of dampers, as long as their force output can be made to be an invertible function of the damper's velocity (either by virtue of their design or by software approach).

It is known from the analysis in Section 3 that the SDA system has shock absorption behavior, which depends on the effective damping constant of the series damper. If the effective damping constant is high, the ability to absorb the impact may be limited. However, in the experimental setup, the MR fluid damper used has an inherent "fuse" torque that limits the torque transmission through it. This provides better impact resistance than the theoretical behavior.

In the experimental setup, we have adopted the digital encoder to indirectly measure the damper input and output velocities. From the two values, the relative velocity in the damper can be computed. Other types of velocity measurement devices can also be adopted for the setup, for example, tachometers, potentiometers, etc. If it is not necessary to measure both the input and output velocities of the damper, we can also have just one velocity sensor to directly measure the relative velocity of the damper. Force sensor may also be incorporated if high force fidelity is desirable. However, this will increase the cost of the overall system.

7. CONCLUSION AND FUTURE WORK

In this paper, the series damper actuator, a novel force/torque control actuator, based on the magneto-rheological fluid damper is introduced. The dynamics of the MR fluid damper is modeled and included into the model of the SDA plant. The force control performance comparison in terms of the bandwidth and output impedance is investigated for the SMRDA and the SNVDA.

A revised Bingham model is proposed to linearize constitutive property of the MR fluid damper. This model has considered the response delay of the MR fluid damper and resulted in a better performance. The overall force control scheme also achieved larger bandwidth. The fixed-end experiment results illustrated that the SDA system could achieve very good output force fidelity. By varying the effective damping constant of the series MR fluid damper, the SDA system is demonstrated to be versatile and applicable for both low- and high-force output.

https://doi.org/10.1017/S0263574706002876 Published online by Cambridge University Press

The performance of inverse dynamics control is usually limited by system hardware limits. The future work would be focused on developing other control algorithm so that a better performance can be achieved. Currently, we are also developing new viscous damper (non-MR-fluid type), which is the desired type of damper for our proposed SDA system. With the new damper, it is believed that the system performance of the SDA system will be further improved.

Acknowledgment

This project is funded by the Academic Research Fund of the National University of Singapore.

References

1. C. M. Chew, G. S. Hong and W. Zhou, "Series Damper Actuator: A Novel Force/Torque Control Actuator," *Proceedings of the IEEE-RAS/RSJ International Conference on Humanoid Robots*, Los Angeles, CA, USA (2004).
2. N. Mandal and S. Payandeh, "Force Control Strategies for Compliant and Stiff Contact: An Experimental Study," *Proceedings of the IEEE International Conference on Systems, Man, and Cybernetics*, San Antonio, Texas, USA (Oct. 2–5, 1994) pp. 1285–1290.
3. S. Sugano, S. Tsuto and I. Kato, "Force Control of the Robot Finger Joint Equipped with Mechanical Compliance Adjuster," *Proceedings of the IEEE International Conference on Intelligent Robots and Systems (IROS)*, Raleigh, North Carolina, USA (1992) pp. 2005–2012.
4. D. W. Robinson and J. E. Pratt, "Series Elastic Actuator Development for a Biomimetic Walking Robot," *Proceedings of the IEEE/ASME Conference on Advanced Intelligent Mechatronics*, Renaissance Atlanta Hotel, Atlanta, Georgia, USA (1999).
5. G. A. Pratt and M. M. Williamson, "Series Elastic Actuators," *Proceedings of the IEEE International Conference on Intelligent Robots and Systems (IROS)*, Pittsburgh, Pennsylvania, USA (1995) pp. 399–406.
6. S. D. Eppinger and W. P. Seering, "Three Dynamic Problems in Robot Force Control," *Proceedings of the IEEE International Conference on Robotics and Automation (ICRA)*, Scottsdale, Arizona, USA (1989) pp. 392–397.
7. M. Zinn, O. Khatib, B. Roth and J. K. Salisbury, "A New Actuation Approach for Human Friendly Robot Design," *Proceedings of the International Symposium on Experimental Robotics*, Italy (2002).
8. C. M. Chew, G. S. Hong and W. Zhou, "Series damper actuator for force/torque control," *US Patent Provisional Application*. Application No.: 60/469, 825.
9. W. Zhou, C. M. Chew and G. S. Hong, "Force control characteristics of series damper actuator," *Internal Report TR-ME-CON-LG003*, Control and Mechatronics Lab., Department of Mechanical Engineering, National University of Singapore, Singapore (2003).
10. N. Takesue, J. Furusho and Y. Kiyota, "Analytic and Experimental Study on Fast Response MR-Fluid Actuator," *Proceedings of the IEEE International Conference on Robotics and Automation (ICRA)*, Taipei, Taiwan (2003) pp. 202–207.
11. N. Takesue, H. Asaoka, J. Lin, M. Sakaguchi, G. Zhang and J. Furusho, "Development and Experiments of Actuator Using MR Fluid," *Proceedings of 2000 IEEE International Conference on Industrial Electronics, Control and Instrumentation*, Nagoya, Aichi, Japan (2000) pp. 1838–1843.
12. J. H. Kim and J. H. Oh, "Design and Analysis of Rotary MR Damper Using Permanent Magnet," *Proceedings of the 2nd IFAC Conference on Mechatronic Systems*, Berkeley, CA, USA (Dec. 9–11, 2002) pp. 899–903.
13. G. Pan, H. Matsuhisa and Y. Honda, "Analytical Model of a Magneto-Rheological Damper and Its Application to the Vibration Control," *Proceedings of the Industrial Electronics Society, IECON 2000, 26th Annual Conference of the IEEE*, Nagoya, Aichi, Japan (2000) pp. 1850–1855.
14. B. F. Spencer Jr., S. J. Dyke, M. K. Sain and J. D. Carlson, "Phenomenological model of a magneto-rheological damper," *J. Eng. Mech., ASCE*, 230–238 (1997).
15. N. Takesue, J. Furusho and M. Sakaguchi, "Improvement of Response Properties of MR-Fluid Actuator by Torque Feedback Control," *Proceedings of the International Conference on Robotics & Automation*, Seoul, Korea (May 21–26, 2001) pp. 3825–3830.
16. W. Zhou, C. M. Chew and G. S. Hong, "Property Analysis for Series MR-Fluid Damper Actuator System," *Proceedings of the IEEE Conference on Robotics, Automation, and Mechatronics (RAM)*, Singapore (Dec. 1–3, 2004).

https://doi.org/10.1017/S0263574706002876 Published online by Cambridge University Press